Measurement of wall shear stress by extended laser-Doppler method using dual spherical waves

by

Katsuaki Shirai[(1)], Shinnosuke Obi[(2)], and Shigeaki Masuda[(3)]

Department of Mechanical Engineering, Keio University,
Hiyoshi 3-14-1, Yokohama 223-8522, Japan

(1) E-mail: td04617@educ.cc.keio.ac.jp
(2) E-mail: obsn@mech.keio.ac.jp
(3) E-mail: smasuda@mech.keio.ac.jp

ABSTRACT

An optical method for measuring the local wall shear stress is considered, that possesses high spatial and temporal resolution, since it serves as an extension of laser Doppler anemometer. The method is based on a technique proposed in the past that utilized the interference of dual cylindrical waves in the wall adjacent region where the direct measurement of velocity gradient at the wall was performed, under the assumption that the velocity increases linearly with the distance from the wall. The technique has been applied to the measurement of turbulent flows and provided a good agreement with the available experiments and direct numerical simulations. The major contribution of the present work is the use of a pair of spherical waves in place of cylindrical waves, aiming at both the improvement of the light-transmission efficiency and the possible extension to two-dimensional measurements. Prior to the application to flow measurement, this paper presents a performance prediction based on optical theories and possible signal processing schema. First, the principle of this method is described, where the interference pattern and the measurement volume are introduced. Then, the Doppler frequency and the signal obtained by this method, as well as a signal processing technique are considered. The result shows that the Doppler frequency of a scattered light by a single tracer particle varies within a burst signal, as a consequence of the change in fringe distance in the measuring volume, and it is found that the extent of frequency variation depends on the direction of tracer particle's path. This suggests the possibility of detecting the direction of the particle path, therefore the direction of the instantaneous local wall shear stress. To detect the frequency variation, a signal processing technique based on Fourier transform is considered, although the proposed technique requires further improvements.

1. INTRODUCTION

Measuring wall shear stress is both important in engineering and in fundamental fluid mechanics research. Many methods for measuring wall shear stress have been proposed (Haritonidis, 1989) and they have achieved some success. Among others, the method based on the velocity gradient at the wall is found to be a compromise of accuracy and generality. However, the velocity measurements in the wall vicinity region are often contaminated by various effects. For example, using hot-wire anemometry (HWA) or laser Doppler anemometry (LDA) is affected by large velocity gradient in the near-wall region of turbulent flows, although some correction methods have been proposed (e.g., Durst et al., 1998). Moreover, it is extremely difficult to determine precisely the distance between the wall and the probe in order to calculate the derivative. The method proposed in the present study is able to evaluate the velocity gradient directly, and it does not require calibration.

An optical method proposed by Naqwi and Reynolds (1984,1991) is a variant of LDA and uses the light interference by a pair of cylindrical waves emitted from the two slits formed on the wall. The method is capable of measuring the instantaneous velocity gradient at the wall without calibration, therefore the direct evaluation of the wall shear stress is possible. Several applications of this technique have been reported so far; Naqwi (1993) reported the performance prediction of the improved method in view of electro-magnetic and scattering theory. He has further improved the robustness by utilizing fiber optics (Naqwi and Petrik, 1993). Obi et al. (1996) applied this method to turbulent flow through a two-dimensional duct. Millerd et al. (1996) improved the robustness by using holography technique. All above researches have used a pair of slits to create cylindrical waves as the original proposal by Naqwi and Reynolds (1984). However, the present authors group has experienced some problems in use of the slit, namely, the transmitting efficiency of the emitting light into the slits is low and it lowers the quality of the signals.

In this work, a pair of pinholes is used in place of the slits. The use of the pinholes resulted in the interference of dual spherical waves whereas the dual cylindrical waves emitted in the case of slit configuration. The transmitting efficiency of light is improved, and hence the quality of the signals during the measurement. The present paper serves for a detailed performance prediction prior to the application to the real flow field. In the subsequent sections, the principles of this method is first described, followed by the prediction with respect to the measurement volume. The dependence of Doppler frequency on the tracer particle's path in the measurement volume is then considered, and consequently a signal processing technique based on Fourier transform will be proposed.

2. PRINCIPLE

The principle of this method consists of linear velocity gradient in the viscous sublayer, interference of dual spherical waves and the Doppler shift by tracer particle. The detailed principle of the method using the interference of two cylindrical waves has been explained in (Naqwi and Reynolds, 1984,1991). In this section, the principle of the method using the interference of two spherical waves is presented in terms of the consideration of the Doppler frequency shift.

The schematic of the flow is depicted in Fig.1, where the definition of the coordinate system is also shown. The wall shear stress is defined by the product of viscous coefficient and velocity gradient of at the wall as:

$$\tau_w \equiv \mu \left. \frac{dU}{dy} \right|_{y=0}, \quad \cdots\cdots (1)$$

where U is the streamwise velocity and y is the axis perpendicular to the wall. The streamwise velocity in the viscous sublayer can be written as the linear function of y,

$$U = C_1 y, \quad \cdots\cdots (2)$$

where C_1 is a constant given as

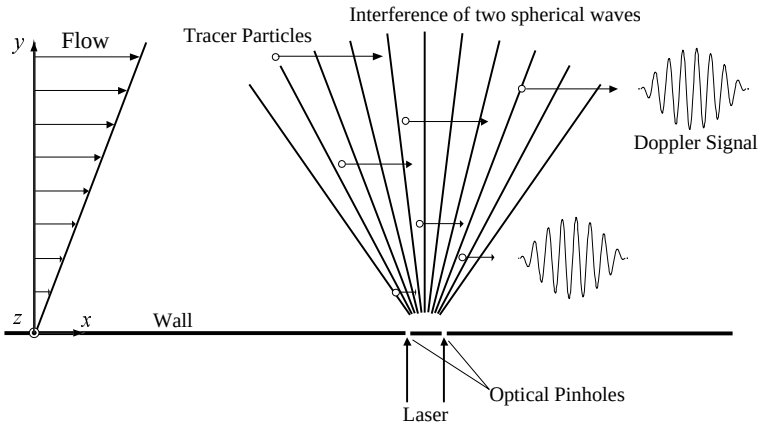

Fig. 1: Schematic of the flow and the principle of the method

$$C_1 = \frac{\tau_w}{\mu} . \quad \cdots\cdots (3)$$

Two optical pinholes are located on the wall and two laser beams are incident on them from behind the wall. The incident laser beams are plane waves, whose wavefront are parallel to the wall, and the beams are diffracted by each pinhole. The diffracted lights are considered as spherical waves emitted from two infinitesimal point sources, provided that the region considered here is in Fraunhofer (far-field) region, i.e., $D<<y$, with D being the distance of two pinholes. When a tracer particle passes through the interference region, the frequency of the scattered light is shifted by Doppler effect. The Doppler frequency is expressed by scalar product (e.g., Durst et al., 1981):

$$f_d = \left| \frac{\mathbf{V}_p \cdot (\mathbf{e}_{1p} - \mathbf{e}_{2p})}{\lambda} \right| \quad \cdots\cdots (4)$$

where $\mathbf{V}_p$ is the velocity vector of the particle passing through the measurement volume, and $\mathbf{e}_{2p}$ and $\mathbf{e}_{1p}$ is the unit vector pointing from each pinhole to the particle as shown in Fig.2. The subscripts 1 and 2 are used for values related to the pinhole located at (-D/2, 0, 0) and (D/2, 0, 0), respectively. The subscript p stands for the particle passing through the measurement volume, and λ for the wavelength of incident laser.

The magnitude of the velocity vector is indicated as V_p and its components are expressed as:

$$\mathbf{V}_p = \begin{pmatrix} V_p \cos\theta \\ 0 \\ V_p \sin\theta \end{pmatrix} . \quad \cdots\cdots (5)$$

Because the normal velocity component is small compared to the other two, it is neglected. θ is the angle of particle velocity shown in Fig. 3 and it is restricted for the range $-\pi/2 < \theta < \pi/2$. When a particle is located at (x_p, y_p, z_p), the unit vectors from each pinhole to the particle is given by

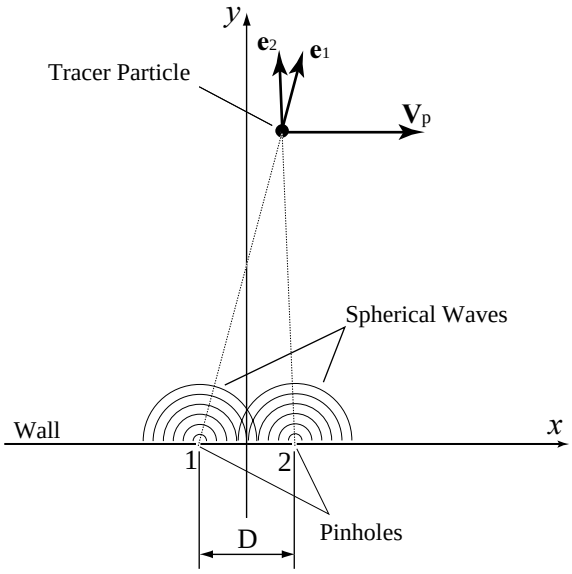

Fig. 2: Doppler effect of tracer particle

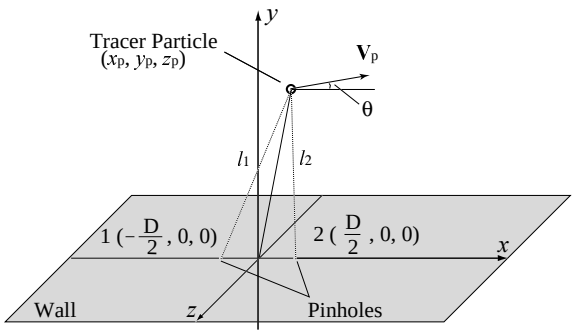

Fig. 3: Trajectory of a tracer particle

$$\mathbf{e}_{1p}=\frac{1}{l_1}\begin{pmatrix} x_p+\frac{D}{2} \\ y_p \\ z_p \end{pmatrix} \text{ and } \mathbf{e}_{2p}=\frac{1}{l_1}\begin{pmatrix} x_p-\frac{D}{2} \\ y_p \\ z_p \end{pmatrix}, \quad \cdots\cdots (6)$$

where l_1 and l_2 are the distance between the particle and each pinhole,

$$l_1=\sqrt{\left(x_p+\frac{D}{2}\right)^2+{y_p}^2+{z_p}^2}\ , \quad \cdots\cdots (7)$$

and

$$l_2=\sqrt{\left(x_p-\frac{D}{2}\right)^2+{y_p}^2+{z_p}^2}\ , \quad \cdots\cdots (8)$$

respectively. Substitution of Eqs. (5) and (6) into Eq. (4), and re-arrangement yields the expression for f_d which can be written as:

$$f_d=\frac{V_p}{\lambda}\left|\left(\frac{1}{l_2}-\frac{1}{l_1}\right)\left(x_p\cos\theta+z_p\sin\theta\right)+\left(\frac{1}{l_1}+\frac{1}{l_2}\right)\frac{D}{2}\cos\theta\right|. \quad \cdots\cdots (9)$$

Under the assumption that the velocity of tracer particle is linear function of y in the viscous sublayer as Eqs.(2) and (3), i.e.,

$$V_p=\frac{\tau_w}{\mu}y\,, \quad \cdots\cdots (10)$$

Eq.(9) can be further arranged to:

$$f_d = \frac{\tau_w y}{\mu \lambda}\left|\left(\frac{1}{l_2}-\frac{1}{l_1}\right)\left(x_p \cos\theta + z_p \sin\theta\right)+\left(\frac{1}{l_1}+\frac{1}{l_2}\right)\frac{D}{2}\cos\theta\right| . \quad \cdots\cdots\cdots\cdots\cdots\cdots\cdots\cdots\cdots\cdots (11)$$

If $\left|x_p \pm D/2\right| << y$ (far-field condition) and the flow is two-dimensional (i.e. the flow is uniform in spanwise direction), Eq. (11) can be reduced to the formula shown by Naqwi and Reynolds (1984, 1991) who have described the prediction method for the dual cylindrical wave case. In this work, a pair of spherical waves is used, so the prediction is needed. To examine the performance prediction accurately, Eq.(11) is invoked in the following session.

3. MEASUREMENT VOLUME

3.1 Interference Pattern

The interference pattern created by dual spherical waves is considered. It is important to know the interference pattern because it helps to predict the Doppler frequency. The three-dimensional interference pattern created by dual spherical waves is depicted in Fig. 4. The spherical waves are originated from two pinholes located on the *x*-axis. The interference pattern is a group of hyperboloids (more strictly, a group of hyperboloids of revolution of two sheets). In contrast to the case of dual cylindrical waves shown in Fig. 5, the pattern of dual spherical waves diverges both in normal and spanwise directions. This divergence in spanwise direction characterizes the difference from the hyperbolic cylinders pattern created by dual cylindrical waves (Fig. 5). The variation of the fringe distance in spanwise location influences the Doppler frequency obtained from particles passing through the measurement volume at different spanwise locations and/or directions.

3.2 Measuring Volume

The measuring volume of the present technique is determined by three independent factors, namely, the dimension and shape of the region of diffracted light, the intensity of light within the interference pattern, and the control volume determined by the receiving optics. The interference pattern is created in the intersecting region of two diffracted lights from two small pinholes. The divergence angle of the diffracted light from a pinhole whose diameter is δ is approximated by:

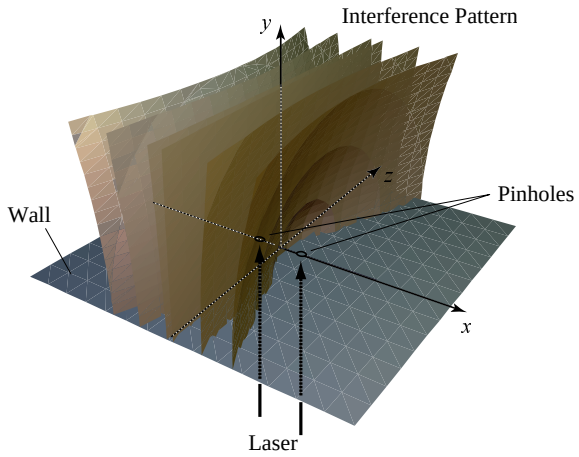

Fig. 4: Interference pattern created by dual spherical waves (hyperboloids)

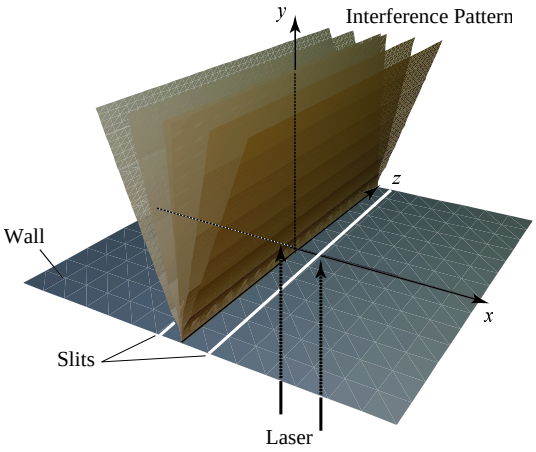

Fig. 5: Interference pattern created by dual cylindrical waves (hyperbolic cylinders)

$$\Delta\alpha \sim \frac{\lambda}{\delta} \quad \cdots\cdots (12)$$

in Fraunhofer (far-field) region. The regions of each diffracted light are given by two cones,

$$\text{light from pinhole1:} \left(x + \frac{D}{2} \right)^2 + z^2 \le r^2 , \quad \cdots\cdots (13)$$

$$\text{light from pinhole2:} \left(x - \frac{D}{2} \right)^2 + z^2 \le r^2 , \quad \cdots\cdots (14)$$

where

$$r = y \tan\left(\frac{\Delta\alpha}{2} \right) + \frac{\delta}{2} . \quad \cdots\cdots (15)$$

Then, the region where interference occurs is the region where these two diffracted lights exist at the same time. It is given by the area which holds above two equations simultaneously and it is depicted in Fig. 6. However, it is yet insufficient to consider the region of diffracted light because the quality of Doppler signals is a function of the light intensity in the measuring volume. It should also be kept in mind that the intensity of the light from each pinhole decreases at the inverse square of the distance from the source. The region detected by the receiver is also to be considered. This depends on the receiving optics used in the measurement; if a lens which has the focal length of f_L is used, the diameter of the region can be approximated as

$$s_L \sim \frac{\lambda}{\Delta\theta} \sim \frac{\lambda f_L}{D_L} , \quad \cdots\cdots (16)$$

where D_L is the diameter of the lens.

As a consequence, the region that satisfies all these three conditions simultaneously determines the measuring volume of this method.

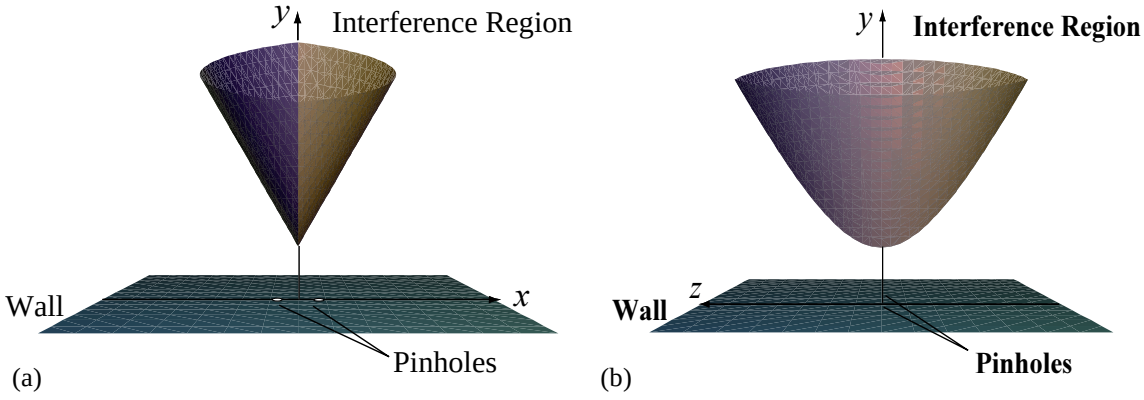

Fig.6: The interference region of dual spherical waves (a) side view, (b) streamwise view

4. PERFORMANCE PREDICTION

As described in the previous section, the interference pattern created by the dual spherical waves has three-dimensionality. The Doppler signal obtained by this method depends on the trajectory of a scattering particle passing the measurement volume. In this section, the Doppler frequency obtained by this method is predicted, and mainly its dependence on the path of particle is considered. The signal processing technique will be discussed in the subsequent section.

4.1 Doppler Frequency Prediction

The Doppler signal by a particle passing the measurement volume is considered as depicted in Fig. 7. In the following, the procedures and the condition for the prediction are described. The position of a particle is a function of velocity V_p and time t,

$$(x_p, z_p) = (V_p t, -V_p t \tan\theta) , \quad \cdots\cdots (17)$$

where the velocity of a particle is already defined by Eq. (10). The range of t is restricted by the particle velocity and the dimension of the measuring volume,

$$-t_{lmt} \le t \le t_{lmt} \quad \cdots\cdots (18)$$

$$t_{lmt} = \frac{x_{lmt}}{V_p \cos\theta} \quad \cdots\cdots (19)$$

where x_{lmt} is determined as the intersecting point of particle and the edge of the measurement volume, cf. Fig. 7:

$$x_{lmt} = \frac{-D + \sqrt{4r^2 - D^2 \tan^2\theta + 4r^2 \tan^2\theta}}{2(1+\tan^2\theta)} . \quad \cdots\cdots (20)$$

The Doppler frequency is determined by Eq. (11) as a function of time. The wall shear stress in Eq. (10) is then estimated by empirical equations in two-dimensional channel flow (e.g., Dean, 1978). The values used in the prediction in this paper is listed in Table1. These values correspond to the case of slit optics (Obi et al., 1996).

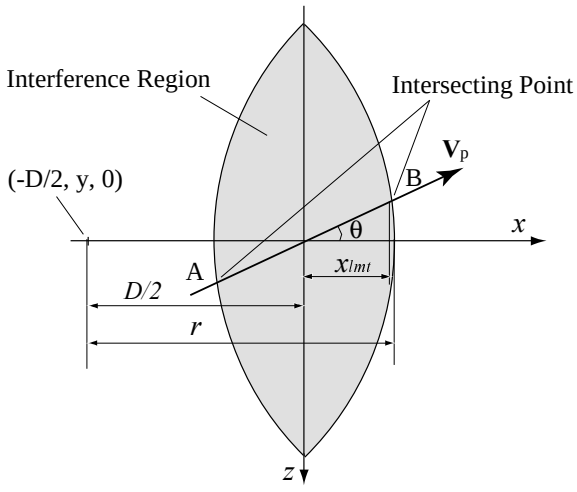

Fig. 7: The trajectory of particle in the measurement volume

Table1: Values used in the prediction

λ	514.5nm
D	11μm
d	1μm
Uc	20m/s
ρ	1.205kg/m^3
μ	18.2 μPa · s

4.2 Effect of Position

The Doppler signal of this method depends on the particle's path, namely, the position and the direction of a tracer particle. In two-dimensional channel flows, the spanwise velocity component is relatively small and may be neglected. However, in this method, the interference pattern diverges in spanwise direction, so the Doppler frequency of the light scattered by a particle would decrease with the increasing spanwise distance of the particle path. The situation is schematically shown in Fig. 8, which is obtained by a prediction using the procedures described in the preceding subsection. It shows the deviation from the constant frequency (red dashed line drawn in Fig. 8) increases apart from x-axis along the span-wise direction. The extent of the deviation is larger near the wall, i.e., for small y.

4.3 Effect of Direction

Next, the influence of the direction of particle on the Doppler frequency is considered. When a particle passes obliquely through the measurement volume, the obtained Doppler frequency varies within a single burst signal. This is another difference from the method using dual cylindrical waves. As the measurement volume of this method located near the center of the xz-plane, most of the signals from tracer particles are obtained near the origin. In this prediction, it is assumed that all the particles pass above the origin of xz-plane, i.e., $(x, z) = (0, 0)$. The time is set to be the range of $-t_{lmt} < t < t_{lmt}$ and the height from the wall is set constant to y = 60 μm, which is within the measurement volume at this flow condition. The predicted frequency is shown in Fig. 9, where the temporal change of frequency is indicated with the direction as a parameter. From the figure, it is seen that the deference of maximum and minimum frequency becomes larger with the increasing angle θ. This implies the possibility of detecting the direction of particle path by detecting the change of the Doppler frequency. However, conventional signal processing techniques for LDA is not directly applicable to this method, because it assumes the frequency in the Doppler signal to be constant within a Doppler burst signal. The present method requires some special ways of signal processing.

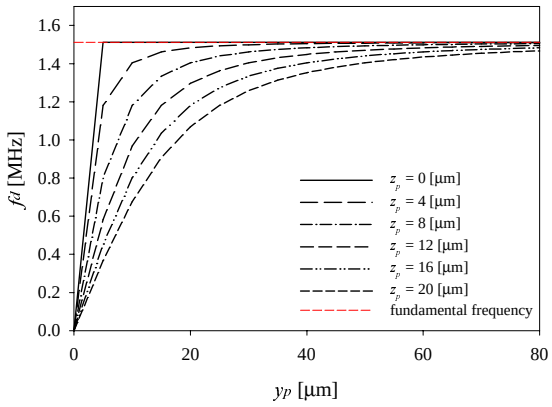

Fig. 8: The frequency dependence of the particle's position

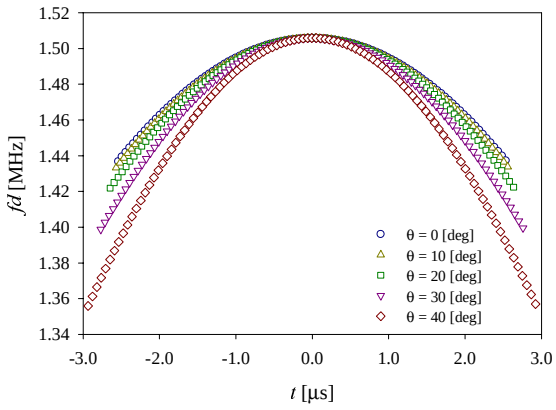

Fig. 9: The frequency dependence of the particle's direction

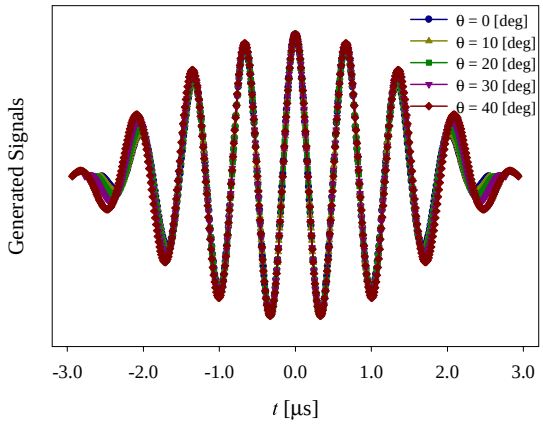

Fig.10: The predicted signals

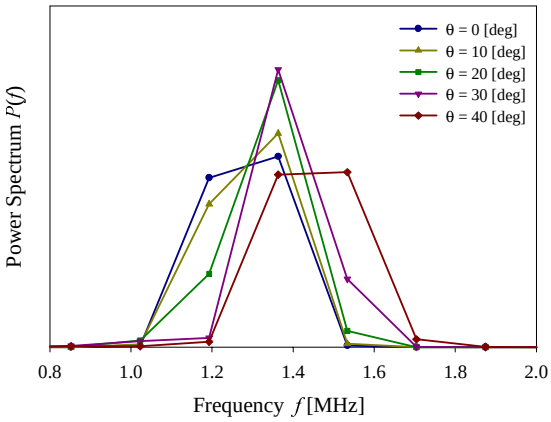

Fig.11: Power spectra of predicted signals

5. SIGNAL PROCESSING

In this section, a signal processing technique for this method is proposed. First, the generation of signals for prediction is explained. Then, the analysis of the signals is done in order to estimate the direction of passing particle in the measurement volume.

5.1 Doppler Signal Generation

The Doppler signal by scattering particle depends on the light intensity eliminated to the particle. The intensity of light in the measurement volume is high in the center than in the edge of the volume. Hence it is considered that the amplitude as well as frequency changes in one Doppler burst signal. Here, the Doppler signal can be written as a function of time

$$S(t) = A(t)\cos 2\pi f_d(t)t\,, \quad \cdots\cdots (21)$$

where f_d is as defined by Eq. (11), and the amplitude is also a function of time:

$$A(t) = \cos 2\pi f_{amp} t\,, \quad \cdots\cdots (22)$$

where the modulation frequency f_{amp} is determined by

$$f_{amp} = \frac{1}{4t_{lmt}}\,. \quad \cdots\cdots (23)$$

The simulated Doppler signals are shown in Fig. 10. The frequency changes slightly with time while the amplitude changes more significantly. In this prediction, a signal is consisted of 512 discrete points, starting at the point A and ending up at B as shown in Fig. 7. It is considered that 512 points are sufficient to avoid aliasing effect in the analysis below.

5.2 Doppler Signal Analysis

The Doppler signal is analyzed with respect to its frequency. To analyze the frequency, N points of signal is

generated in the range ($-t_{lmt} < t < t_{lmt}$) by the procedures above. Then the generated signals are analyzed by the discrete Fourier transform and it's power spectrum is calculated by

$$F(f)=\sum_{n=0}^{N-1} S(t)\exp\left(-j\frac{2\pi fn}{N}\right) \quad \cdots\cdots (24)$$

$$P(f)=\frac{F(f)\cdot F^{*}(f)}{N}, \quad \cdots\cdots (25)$$

where N is the number of samples and superscript * denotes complex conjugate. The result is shown in Fig. 11 for different angles of particle path. It shows the data with finite value are few, and it is not plausible that the passing angle can be detected from this raw power spectrum.

5.3 Signal Processing

The following gives a signal processing technique for the determination of frequency change and direction of particle trajectory. To detect the latter, the suitability of the width of interpolated power spectrum function is investigated as an indication of the frequency variation within a burst signal.

As already pointed out, the number of data points is not sufficient to evaluate the width of power spectrum function, so the interpolation is performed by Gaussian distribution. In order to obtain better fitting, the raw power spectrum data is converted to natural logarithmic scale before Gauusian fitting. In logarithmic scale, Gaussian distribution is expressed by a parabolic function,

$$\log P(f)=af^{2}+bf+c. \quad \cdots\cdots (26)$$

The approximation was done by least-square fit for four data points that are selected by extracting four largest data points of power spectrum while eliminating data points with extremely small values. The parabolic fit data are depicted in Fig. 12 with reduced power spectrum data. The width of the function is measured by broadening factor (=B.F.) which corresponds to the standard deviation of Gaussian distribution

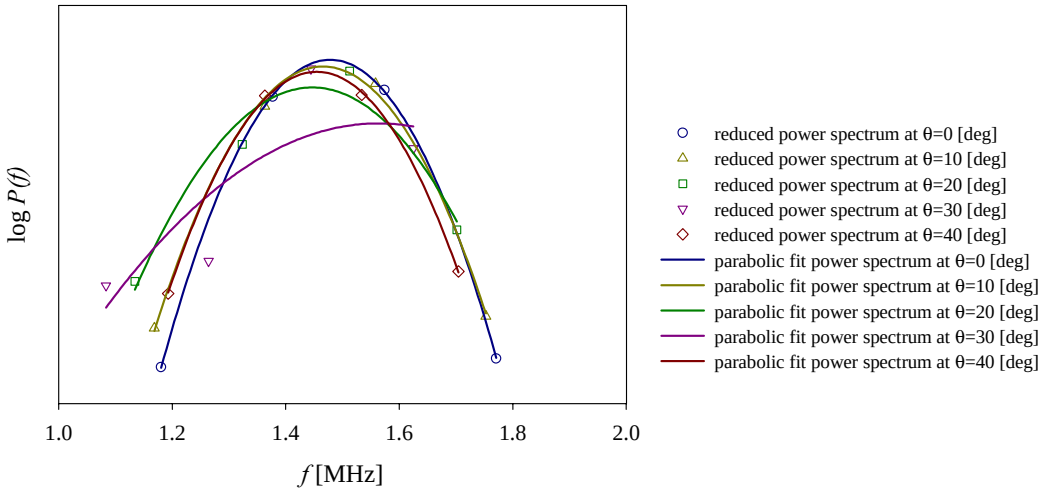

Fig. 12: Reduced and parabolic fit power spectrum

Table 2: Particle's path angle and broadening factor of power spectrum

θ (deg)	Broadening Factor
0	0.09
10	0.10
20	0.12
30	0.19
40	0.09

$$\text{B.F.}=\sqrt{-\frac{1}{2a}}\ . \qquad (27)$$

The obtained values of broadening factor are summarized in Table 2. It has been expected to show the distribution of the spectrum becomes wider as the angle θ increases, and this is confirmed by the broadening factors in Table 2 except for the case of θ = 40 deg. However, this is not sufficient to detect the accurate direction of passing particle due to the small amount of original data points. The possible reason for this is the lack in resolution in frequency domain: The resolution of frequency is determined by the residential time of the signal, t_{lmt}, and this restriction of time and frequency resolution is generalized by the Heisenberg uncertainty principle. The signal processing technique presented above is not sufficient for detecting the angle of particle trajectory as long as the residential time of signal is restricted. Other techniques for this purpose must be introduced. Short time Fourier transform or wavelet analysis may be the next candidates.

6. SUMMARY

In this paper, a new optical measurement method for local shear stress using dual spherical waves was presented, that is an extension of laser Doppler anemometry. This paper presents detailed performance prediction prior to the actual flow measurement. First, the principle was described with linear velocity gradient in viscous sublayer, interference of two spherical waves and Doppler shift frequency, followed by the prediction of the interference pattern used in this method and the measuring volume. Then, the Doppler frequency of a scattered light by a single tracer particle is estimated with respect to particle's path. The results show the Doppler frequency changes in a burst signal, which depends on the particle's path in the measuring volume. This implies possibility of detecting the direction of the particle and hence the direction of the instantaneous local wall shear stress. To detect the frequency variation, a signal processing technique based on Fourier transform was presented, although it is not sufficient to achieve the precise detection of direction and some future improvements are required.

REFERENCES

Dean, R. B. 1978 Reynolds number dependence of skin friction and other bulk flow variables in two-dimensional rectangular duct flow, *Trans. ASME J. Fluid Eng.* **100**, 215-223.

Durst, F., Fischer, M., Jovanović, J. and Kikura, H. 1998 Methods to set up and investigate low Reynolds number, fully developed plane channel flow, *Trans. ASME J. Fluid Eng.* **120**, 496-503.

Durst, F., Melling, A. and Whitelaw, J. H. 1981 *Principles and Practice of laser-Doppler Anemometry*, Academic Press.

Haritonidis, J. H. 1989 The measurement of wall shear stress, in *Advances in Fluid Mechanics Measurements*, Lecture Notes in Engineering 45, edited by C. A. Brebbia, S. A. Orszag and M. Gad-el-Hak, Springer Verlag, 229-261.

Millerd, J. E., Swienton, J. P., Unterscher, F., Trolinger, J. D., Smith, L. G. and LaRue, J. C. 1996 Holographic sensor for measurement of wall velocity gradients, *Exp. Fluids* **21**, 469-476.

Naqwi, A. A. 1993 Performance prediction of dual cylindrical wave laser devices for flow measurements, *Exp. Fluids* **14**, 121-132.

Naqwi, A. A. and Petrik, S. 1993 Fiber-optic dual-cylindrical wave sensor for measurement of wall velocity gradient in a fluid flow, *Appl. Optics* **32**, 6128-6131.

Naqwi, A. A. and Reynolds, W. C. 1984 Dual cylindrical wave laser-Doppler method for measurement of wall shear stress, in *Laser Anemometry in fluid mechanics - II*, edited by R. J. Adrian, D. F. G. Durão, F. Durst, H. Mishima and J. H. Whitelaw, LADOAN-Instituto Superior Técnico, Lisbon Portugal, 105-122.

Naqwi, A. A. and Reynolds, W. C. 1991 Measuring of turbulent wall velocity gradients using cylindrical waves of laser light, *Exp. Fluids* **10**, 257-266.

Obi, S., Furukawa, T. and Masuda, S. 1996 Experimental study on the statistics of wall shear stress in turbulent channel flows, *Int. J. Heat and Fluid Flow* **17**, 187-192.